Extended Abstracts of the 2010 International Conference on Solid State Devices and Materials, Tokyo, 2010, pp487-488

Monolithic Integration of Ni-SPC Poly-Si TFTs and Lateral Large-grained Poly-Si TFTs

Akito Hara, Kenji Kondo, Tsutomu Sato and Tadashi Sato

Department of Electronic Engineering, Tohoku Gakuin University, 13-1 Chuo-1, Tagajo 985-8537, Japan
Phone:+81-22-368-7282 E-mail: akito@tjcc.tohoku-gakuin.ac.jp

1. Introduction

Nickel (Ni)-induced solid-phase crystallization (Ni-SPC) is an attractive method for forming a poly-Si film on a glass substrate at low temperatures (<600°C) [1,2]. Ni-SPC poly-Si thin-film transistors (TFTs) exhibit an on-current that is sufficiently high for them to be used in the backplane of an OLED. Monolithic integration of Ni-SPC poly-Si TFTs and lateral large-grained poly-Si TFTs on a glass substrate can serve to realize a novel "system-on-glass" (SoG) (Fig. 1). In the SoG described in this paper, a lateral large-grained poly-Si film is selectively grown via irradiation using a diode-pumped solid-state (DPSS) continuous wave (cw) green laser [3–5] on a predetermined region of an Ni-SPC poly-Si film, where the peripheral circuit of the SoG is fabricated. In this paper, the two types of TFTs mentioned above were fabricated on different regions of a glass substrate, and then, the performance of each was evaluated.

2. Experiments

The Ni-SPC poly-Si film was fabricated by depositing a thin layer of Ni onto a 100-nm-thick a-Si film on a non-alkaline glass substrate, followed by annealing at 580°C for 6 h. The concentration of Ni in the Ni-SPC poly-Si film was determined as 5×10^{18} cm^{-3} by secondary ion mass spectroscopy (SIMS) (Fig. 2). To evaluate the performance of the two types of poly-Si TFTs, two poly-Si regions with different crystalline qualities were fabricated on a glass substrate. Half of the substrate is made up of the Ni-SPC poly-Si film and the other half is made up of the lateral large-grained poly-Si film; the latter is prepared by irradiating a DPSS cw green laser on the initial Ni-SPC poly-Si film (Fig. 3).

Figure 4 outlines the TFT fabrication processes. Following the formation of islands of poly-Si by reactive ion etching, 50-nm-thick gate SiO_2 layers were deposited by PECVD at 325°C using SiH_4 and N_2O. Then, Mo was sputtered as the gate metal. Ion implantation (2×10^{15} cm^{-2} at 10 keV) was used to form the S/D region. This region was activated by annealing at 550°C for 6 h in N_2, and an SiO_2 interlayer was deposited by PECVD at 325°C. Finally, the drain metal (Mo) was deposited by sputtering. Hydrogenation annealing was performed in hydrogen gas (H_2:Ar = 3:97) at 400°C. Figure 5 shows a photograph of the Ni-SPC poly-Si TFT fabricated by this process.

3. Results

Figure 6 shows the crystalline quality of the two different poly-Si regions. The grain size of the Ni-SPC poly-Si film is very small and a high concentration of defects is visible (Fig. 6(a)). On the other hand, the grain size of the lateral large-grained poly-Si film is very large and is around 1×10 μm^2 (Fig. 6(b)).

The behavior of the Ni impurities in the lateral large-grained thin poly-Si film was studied by carrying out thermal annealing at 580°C for 6 h to simulate the thermal budget of the poly-Si TFT process. The plane-view STEM image of this film (Fig. 7(a)) shows that large and good-quality grains are formed in the film. A dark structure is observed at the triple junction. Figure 7(b) shows the results of the STEM-EDX analysis of this junction region and of the in-grain regions; it is clear from this figure that the Ni impurities are aggregated in the dark structure. Figure 8 shows electron diffraction (ED) patterns recorded at different points in the dark structure and reveals that the structure consists of a single $NiSi_2$ crystal.

Figures 9(a) and (b) show the transfer and output characteristics of the two types of TFTs. The lateral large-grained poly-Si TFTs and the Ni-SPC poly-Si TFTs respectively have large and small on-current and small and large s-value. It is noteworthy that the off-current of the former is very large as compared to that of the latter. Table I summarizes mobility of the TFTs.

4. Discussions

Figure 10 shows the different stages in the formation of $NiSi_2$. The dark structure is not observed after laser recrystallization, indicating that $NiSi_2$ is formed in our simulation annealing at 580°C for 6 h. Immediately after laser recrystallization, the Ni impurities become dispersed in the large-grained poly-Si film (Fig. 10(a)). Because the diffusion coefficient of the interstitial Ni impurities is very large at around 580°C [6,7], the grain boundaries act as effective gettering sites (Fig. 10(b)). After gettering at the grain boundaries, the Ni impurities diffuse along the boundaries, become trapped at the triple junctions (Fig. 10(c)), and are finally converted to $NiSi_2$ (Fig. 10(d)).

Lateral large-grained poly-Si TFTs have a high mobility because of the low concentration of carrier scattering centers. The small s-value is also consistent with the high quality of large-grained poly-Si films. These characteristics might imply that the off-current of a lateral large-grained poly-Si film should be low. However, a large off-current was observed in lateral large-grained poly-Si TFTs. When metallic particles of $NiSi_2$ are formed in the drain junction region, they act as leakage sites, resulting in a large off-current. On the other hand, an Ni-SPC poly-Si film consists of small grains and has a high concentration of defects. Thus, Ni impurities in these films are dispersed into a high concentration of defects, and consequently, Ni does not grow to form large metallic $NiSi_2$ particles. Thus, Ni-SPC poly-Si TFTs have a low off-current.

5. Conclusions

The monolithic integration of Ni-SPC poly-Si TFTs and lateral large-grained poly-Si TFTs on a glass substrate allows the realization of a novel SoG. In this paper, the monolithic integration of both types of TFTs on a glass was achieved, and the performance of both TFTs was evaluated. A larger field-effect mobility was obtained for the lateral large-grained poly-Si TFTs than for Ni-SPC poly-Si TFTs. However, the off-current of the former was larger than that of the latter. This results from the formation of metallic $NiSi_2$ particles at the triple boundary junction in lateral large-grained poly-Si film; these particles subsequently act as leakage sites under a strong electric field at the drain junction.

Acknowledgement

This study was supported in part by a Grant-in-Aid for Scientific Research (B, 19360165 and C, 22560341) from the Japan Society for the Promotion of Science.

References

[1] R. C. Cammarata et al.: J. Mater. Res. 5 (1990) 2133.
[2] C. Hayzelden et al.: J. Appl. Phys. 73 (1993) 8279.
[3] A. Hara et al.: Dig. Tech. Papers of the Int. Workshop on 2001 AM-LCD -TFT Technologies and Related Materials, Tokyo, 2001, p. 227.
[4] A. Hara et al.: IEDM Tech. Dig., 2001, p. 747.
[5] A. Hara et al.: Jpn. J. Appl. Phys. 43 (2004) 1269.
[6] G. W. Ludwig et al.: Solid State Phys. 13 (1962) 223.
[7] E. R. Weber: Appl. Phys. A30 (1983) 1.

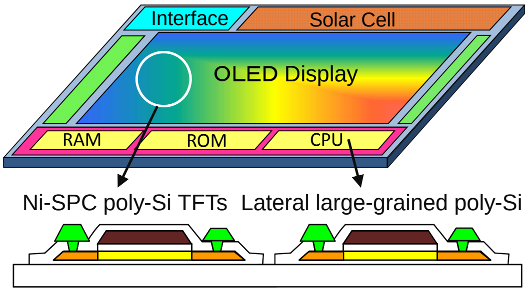

Fig. 1. System on glass (SoG) fabricated using Ni-SPC poly-Si TFTs and lateral-large-grained poly-Si TFTs.

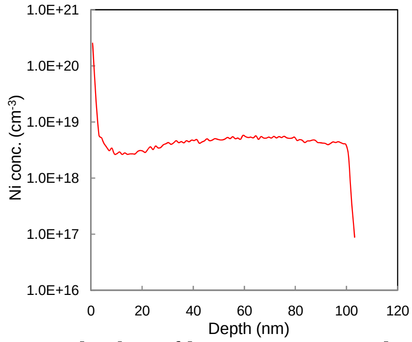

Fig. 2. Ni depth profile in an Ni-SPC poly-Si film

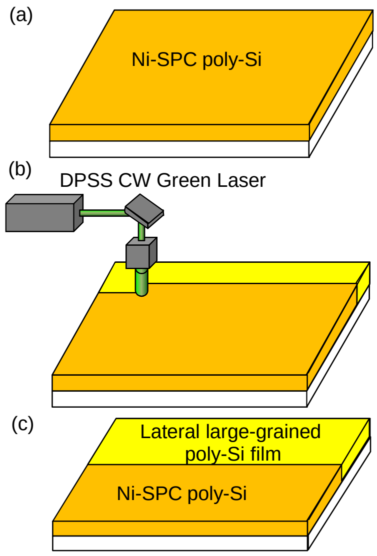

Fig. 3. Monolithic integration of two types of poly-Si films

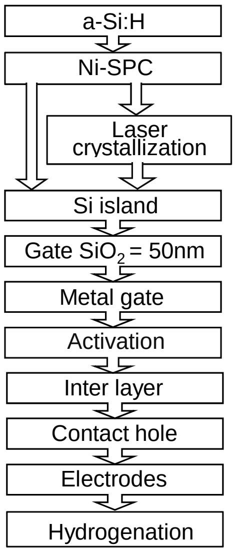

Fig. 4. Device fabrication processes

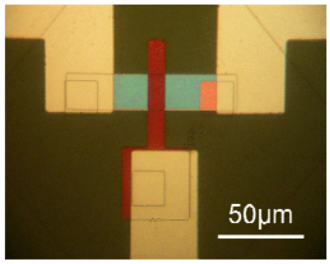

Fig. 5. Photograph of fabricated poly-Si TFT

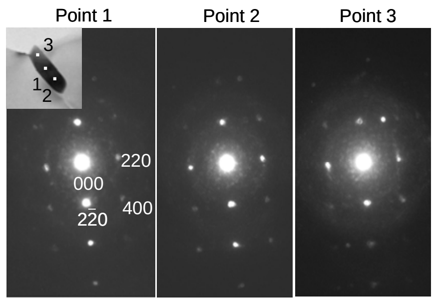

Fig. 8. ED pattern of three different points in dark structure

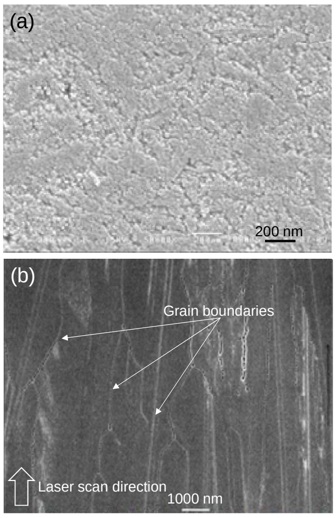

Fig. 6. FE-SEM images of (a) Ni-SPC poly-Si and (b) lateral large-grained poly-Si film

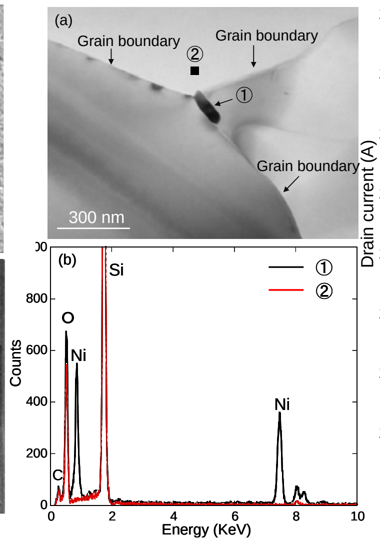

Fig. 7. (a) STEM image of lateral large-grained poly-Si film and (b) EDX of two regions.

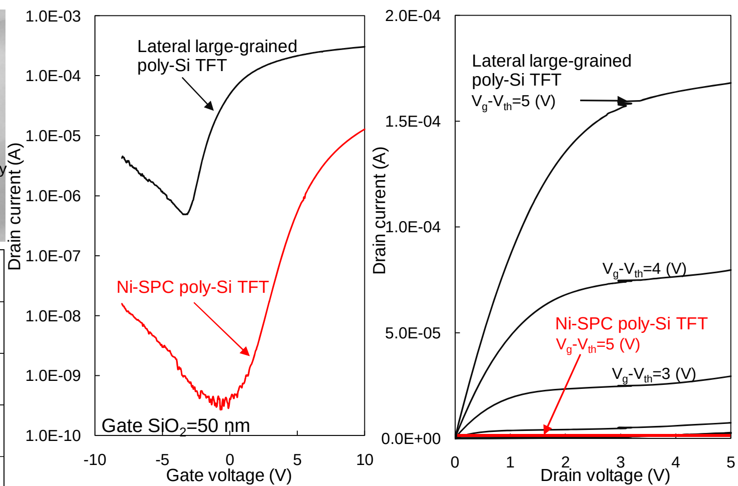

Fig. 9. Performance of Ni-SPC poly-Si TFT and lateral large-grained poly-Si TFT

Table I. Performance of TFTs

	Ni-SPC poly-Si TFT	Lateral large-grained poly-Si TFT
Field-Effect Mobility (cm^2/Vs)	28	283

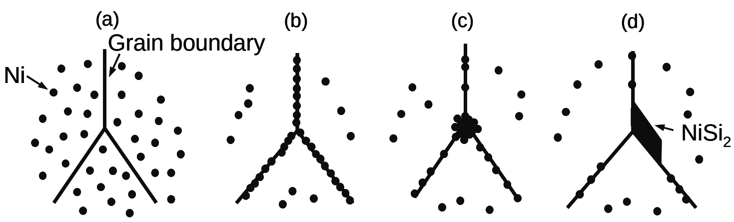

Fig. 10. Formation mechanism of $NiSi_2$